# Metasurface-Enabled Circular Light Propagation for Ultra-fast and Efficient Photodetection

M Saif Islam<sup>1</sup>, Amita Rawat<sup>1</sup> and Makoto Tsubokawa<sup>2</sup>

<sup>1</sup>Department of Electrical Engineering Computer Science, University of California – Davis, Davis, California, 95616, USA

<sup>2</sup>Graduate school of Information, Production, and Systems, Waseda University, 2-7 Hibikino, Wakamatsu, Kitakyusyu, 808-0135, Japan.

#### **ABSTRACT**

We present a novel photodetector concept that involves the metasurface-induced scattering of a vertically incident photon beam wave front toward desired direction, facilitating guided light propagation, and resulting in enhanced detection efficiency in an ultra-thin photo absorption layer. The higher absorption efficiency is enabled by an enhanced photon density of states while substantially reducing the optical group velocity of light and extending the photon material interaction time compared to the traditional semiconductor photodetectors without an integrated metasurface. We have demonstrated a surface-illuminated Si PIN photodiode (PD) structure with a metasurface composed of etched isosceles triangle pillars using Finite Difference time Domain numerical simulation that can enable photon beam steering and guided light propagation. This increases the absorption efficiency in devices with very small diameter (<10µm), surpassing the capabilities of conventional omnidirectional scattering diffraction patterns. Our results show a 3.5-fold increase in internal quantum efficiency over wavelengths above 900 nm compared to the structure without metasurface. The absorption enhancement brought about by directional scattering is not limited to thin i-layers; it can potentially improve a wide range of photodiode geometries and structures.

Keywords: High-speed photodetectors, speed-efficiency trade-off, metasurface, circular light propagation

#### 1. INTRODUCTION

Photon trapping structures address the bandwidth-efficiency trade-off in photodetectors (PD) by enhancing the light-matter interactions <sup>1-4</sup>. Periodic arrays of micro and nanoscale surface structures are used to bend normally incident beams of photons into laterally propagating modes along the plane of semiconductor films <sup>4-7</sup>. Such structures bend light beams, slow them down, and contribute to unprecedented improvement in the light absorption efficiency in devices, even when designed with ultra-thin absorption regions. However, maximizing their efficiency in ultrafast devices remains a challenge due to a multitude of factors influencing their design and fabrication. An ultrafast PD is designed to be small in area with a typical diameter of ~10μm and with a thin absorption layer thickness to enable low RC time and short transit time. Since wavelengths close to the bandgap of semiconductors always exhibit low absorption coefficients, such small diameters are not sufficient for absorbing propagating modes along the plane of semiconductor films. For example, at 850 nm, we need around 23μm absorption length to absorb >90% of the photons in silicon. Detecting such long wavelengths are important for many ongoing and emerging applications in optical communications, sensing, or imaging <sup>7-13</sup>.

Further author information: (Send correspondence to M Saif Islam and Makoto Tsubokawa)

Makoto Tsubokawa, E-mail: tsubokawa.m@waseda.jp

Amita Rawat, E-mail: famita@ucdavis.edu M Saif Islam, E-mail: sislam@ucdavis.edu Here, we propose a strategy to improve the photon trapping effect in devices with small areas by redirecting the vertical incident wavefront and guiding it circularly to ensure speed of operation while increasing the photon absorption efficiency. We will use silicon to demonstrate the concept and show that near-infrared (NIR) detection efficiency can be considerably increased while ensuring ultrafast operations.

## 2. PROPOSED DEVICE DESIGN

External Quantum Efficiency (EQE) is one of the key parameters that describe the sensitivity of PDs. We have designed and fabricated several photon trapping (PT) PDs with integrated surface structures (nanoholes) by varying the nanohole dimensions (diameter and period) and number of nanoholes (N). We also studied the influence of the N on the measured EQE, where a set of devices with a constant device D of  $50~\mu m$  is characterized. SEM images of such devices with different N are illustrated in Figure 1a. The measured EQE is presented in Figure 1b for PT PDs with a fixed nanohole period and diameter of 1000 and 700 nm, respectively, for hexagonal lattice and inverted pyramid profile on SOI substrate, where the N is varied from 0 (control) to 820. Compared to the control device with an EQE of  $\sim 12\%$ , the EQE of the PT devices gradually increases with increasing N, exhibiting a maximum of >38% for an N value exceeding 820. This experiment mainly demonstrates a correlation between the EQE of a photodetector and N  $^1$ . The EQE enhancement observed in the device is due to the improved coupling of vertically incident light into laterally propagating modes with increasing N within the same area of the devices. We also found that an increase in the planar area in a device, such as  $100\mu m$  or  $250\mu m$  diameters, leads to higher absorption in the photoactive layer  $^{1,10,14,15}$ . Consequently, the overall EQE of the PT devices is increased to more than 80% in comparison to the control device  $^{1,6}$ . This observation indicates that as device areas are reduced, the benefits of traditional PT techniques cannot be fully realized.

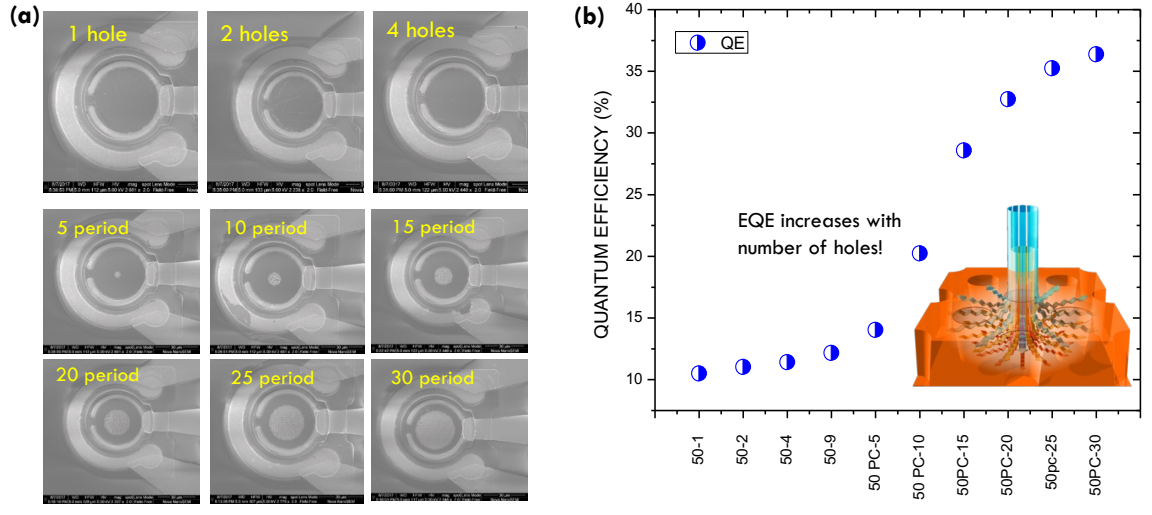
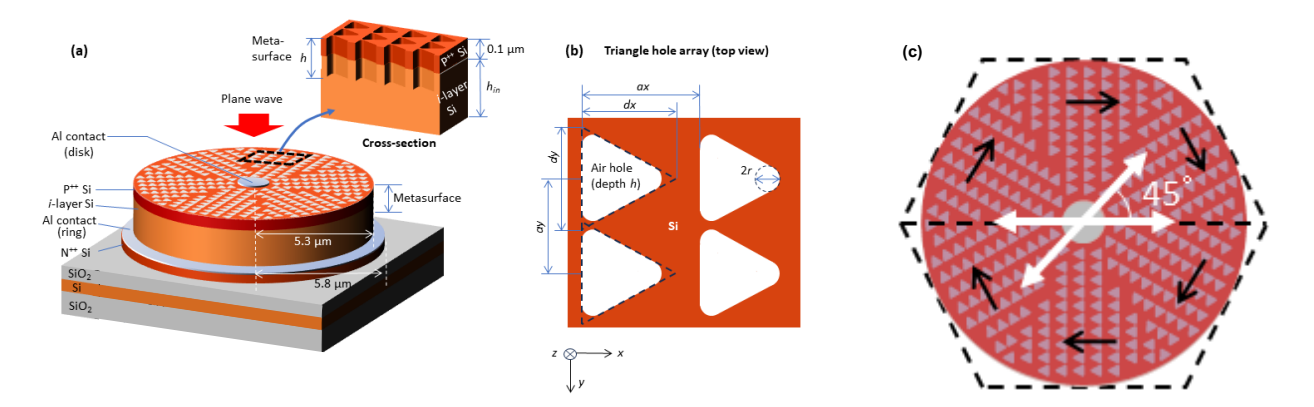


Figure 1. External Quantum Efficiency (EQE) versus number of nanoholes (N) in PDs under 850 nm laser illumination. (a) SEM images of PDs with an increasing N in devices with 50  $\mu$ m diameter. (b) Fitted curve shows that EQE starts with ~12% efficiency for control PD (no photon-trapping structures) and saturates at ~38% for photon-trapping (PT) PD with ~30 periods of PT nanoholes. This observation indicates that as device areas are reduced, the benefits of traditional PT techniques cannot be fully realized due to the limited lateral propagation path length. The inset shows a vertically oriented photon beam diffracted into laterally oriented omnidirectional guided modes in a PT semiconductor photodetector.

In this study, we considered metasurfaces with wavefront deflection function instead of a periodically etched surface structure to improve the sensitivity in long wavelengths. Due to the sub-wavelength size and periodic arrangement of shape, these metasurfaces work as meta-atomic elements and enable phase control instead of simple scattering of incident light. Several groups reported metasurfaces enabled for beam deflection in active devices such as photodetectors <sup>16-20</sup>. We used isosceles triangle hole arrays with a period of approximately one wavelength. Because the distance between the two sides

of an isosceles triangle varies continuously in the apex direction, multiple spatial mode excitations necessary for beam deflection can be expected. Additionally, these metasurfaces also result in enhanced absorption electromagnetic (EM) wave absorption based on directional scattering (DS) of photons, contributing to longer absorption length without increasing absorption layer thickness.



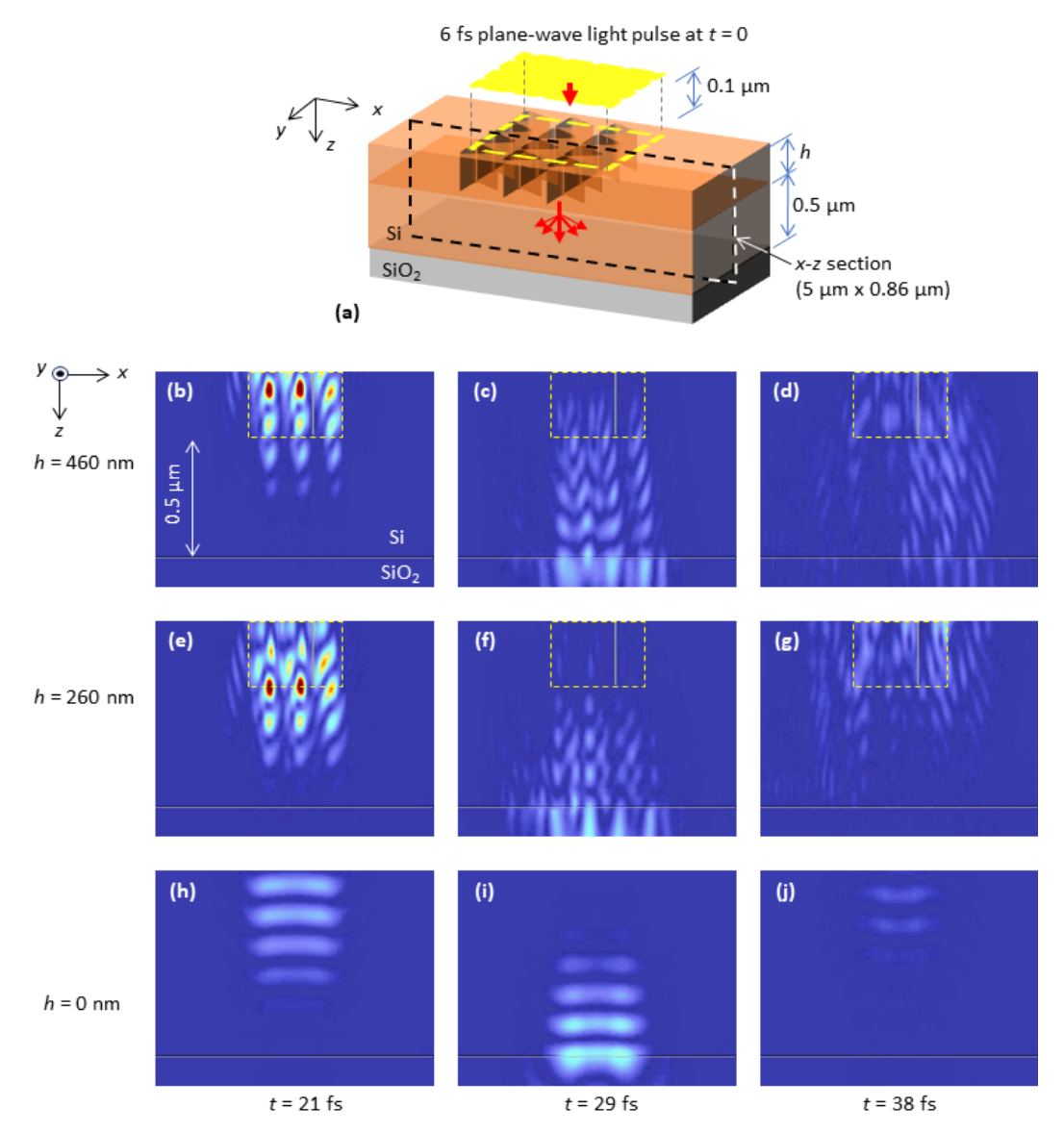
**Figure 2.** Schematic of the simulated PD structure with metasurface. (a) Perspective view. Triangular holes can be etched on the surface to reach the i-layer of the device. At the bottom, there is  $N^{++}$  contact layer. (b) Top view of part of the triangular hole array. For ease of fabrication, the vertices are rounded with radius r. The vertex directions of the isosceles triangles are aligned with the direction of the hexagonal sides inscribed in the top-layer circle. (c) The vertex directions (black arrows) of the isosceles triangles are parallel to the sides of the circumscribed hexagon (dotted line), and  $0^{\circ}$  coincides with one of them.

Figure 2(a) shows a perspective view of the proposed photodetector (PD) structure, which features a metasurface on top. The structure consists of a top layer made of heavily doped P++ silicon, sitting on an intrinsic silicon (i-layer) below. The metasurface has isosceles triangle-shaped holes etched through these two layers. As shown in Figure 2(b), these holes are arranged in a two-dimensional array, all oriented in the same direction, with periods  $a_x$  and  $a_y$ . The vertices of the triangles are rounded with a 50-nanometer radius to make fabrication easier. Figure 2(c) shows the vertex directions (black arrows) of the isosceles triangles that are parallel to the sides of the circumscribed hexagon (dotted line).

The shapes of the isosceles triangles vary with respect to the direction of their apex, meaning the distance between the two sides changes gradually, which creates different spatial optical modes at various positions within a triangle. These phase differences between the modes are generated within one grating period, and a series of phase differences between adjacent gratings deflect the transmitted light. The appropriate phase difference for deflection is influenced by the triangles' geometry, lattice period, etch depth, and optical wavelength. Our design was inspired by previous studies <sup>16,17</sup> that explored the sizes of cylindrical and quadrilateral pillar arrays to determine the optimal size of triangular prisms.

#### 3. DISCUSSION

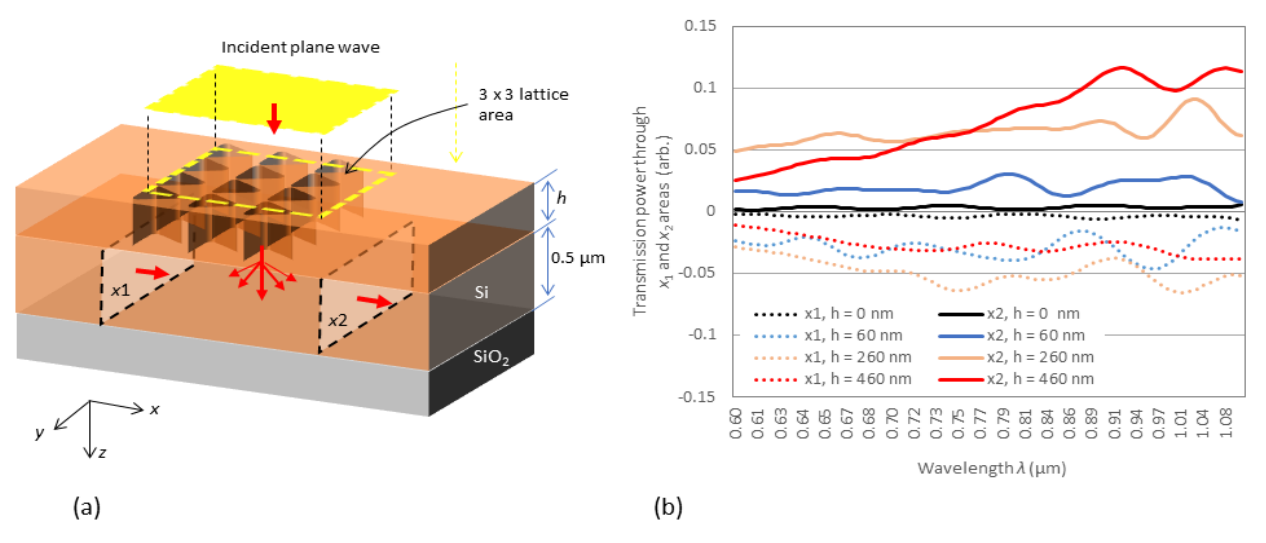
The light propagation and absorption properties in the proposed PD structures were calculated using the Lumerical FDTD solver. To verify the deflection effect in detail, the *E*-field intensity propagation in the *x-z* cross section was investigated using a partial model of  $3 \times 3$  nanohole lattices (Figure 3(a)). Here, the thickness of the Si layer below is kept constant at 0.5  $\mu$ m. The 45° linearly polarized light pulse of  $\lambda_c = 0.9 \mu$ m,  $\Delta \lambda = 0.1 \mu$ m, and ~6 fs long emitted at t = 0 is incident on the top surface. Figures 3(b)–4(j) show the *E*-field intensity variation at 21 fs, 29 fs, and 38 fs time stamps. The *x*- and y-axes of the monitor cross section is 5  $\mu$ m long and 0.86  $\mu$ m deep (i.e., SiO<sub>2</sub> base 0.1  $\mu$ m, *i*-layer 0.5  $\mu$ m, meta-surface 0.26  $\mu$ m). We can see in Figs. 3(b)–3(d) that at h = 460 nm the optical pulse is slightly deflected and propagates in the right side direction of the figures (+*x* direction) and is reflected from the SiO<sub>2</sub> boundary in the upper right direction. On the other hand, at h = 260 nm, multiple diffracted pulses are also generated, but the propagation is almost symmetrical. These field intensity patterns are not simply deflected plane wave propagation due to the superposition



**Figure 3.** (a) 3 × 3 periodic nanohole piece model; a light pulse with 45° linear polarization normally illuminates only the metasurface piece section (approx.  $0.17 \mu m \times 0.13 \mu m$ ). The black dashed line is a monitoring plane (5 μm ×  $0.86 \mu m$ ) of the E-field intensity, covering from the meta surface to the SiO<sub>2</sub> substrate. The cross-section is located between triangular holes. Non-reflective Perfectly Matched Layer (PML) conditions are added to both the x- and y-direction end faces and to the SiO<sub>2</sub> bottom surface. (b)–(d) E-field intensity transitions at times 21, 29 and 38 fs after incidence for the case of h = 460 nm. Dashed lines indicate metasurface positions. (e)–(g) for h = 260 nm. (h)–(j) for h = 0 without metasurface.

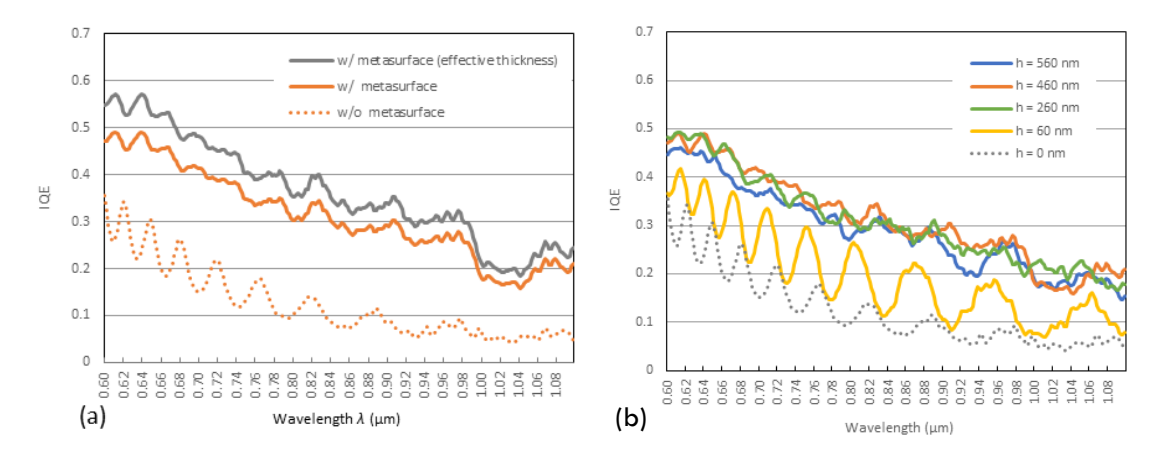
of some diffraction order lights with different amplitudes and phase distortions. The tringle array is designed to maximize the total diffracted wave component in the +x direction. For reference, without metasurfaces, as seen in Figs. 3(h)–3(j), the diffraction effect is small, resulting in almost plane wave propagation. Furthermore, using the same model shown in Fig. 3(a), the deflection characteristics as a function of metasurface thickness h is evaluated from the power flow passing through the  $x_1$  and  $x_2$  cross-sections. Detailed dynamics of the power flow are presented in Ref 22.  $^{21}$ 

Figure 4 shows, at  $h = 0.46 \mu m$ , the transmitted power of  $x_2$  is significantly larger than that of  $x_1$ , indicating that the +x direction flow dominates in the longer wavelength region; however, when h is halved, it diffracts almost equally in both directions. Furthermore, as h approaches 0, the deflection effect almost disappears.



**Figure 4**: Light deflection manipulation with metasurface thickness h. (a) Same model as Fig. 3(a). The light power transmitted through  $x_1$  and  $x_2$  of the y-z cross-section in the Si layer is monitored. (b) Transmitted cross-sectional power as a function of h. The sign of the  $x_1$  transmitted light is negative because of the direction of the inflow.

Figure 5(a) shows the simulated internal quantum efficiency (IQE). The thicknesses of the metasurface h and i-layer  $h_{in}$  are 0.46 and 1  $\mu$ m, respectively. The orange solid and dotted lines represent the IQE values with and without the metasurface, respectively. The gray line indicates the orange line divided by the i-layer effective thickness, which reflects the absorption efficiency per Si unit volume of the i-layer. We can see that the absorption within the Si bulk is improved by  $\sim$ 10%. Figure 5(b) shows the IQE spectra for different etch depths, i.e., the metasurface thickness h. The IQE trend in



**Figure 5.** (a) Internal Quantum Efficiency (IQE) spectra for 1- $\mu$ m i-layer and 0.46- $\mu$ m metasurface. (a) IQE with and without metasurface. The gray line indicates the IQE for the effective thickness. (b) Etch depth h dependence of IQE. The thicknesses of P<sup>++</sup> and i-layers are fixed at 0.1 and 1  $\mu$ m, respectively. h = 0 indicates a flat surface with no metasurface.

the long wavelength region nearly saturates at 4× enhancement for 0.26  $\mu$ m  $\leq h \leq$  0.56  $\mu$ m with a maximum IQE at around  $h = 0.46 \mu$ m compared to h = 0 nm and shows  $\sim$ 2× IQE enhancement for  $h < 0.26 \mu$ m with respect to h = 0 nm.

In photon-trapping photodetectors, a large planar area is advantageous for achieving high absorption efficiency, particularly when dealing with wavelengths close to the semiconductor's bandgap. This efficiency arises from the weak absorption coefficients associated with these wavelengths, necessitating extended lateral propagation to absorb the incident photons effectively. However, the design of ultrafast photodetectors typically involves minimizing the device area to enhance speed and response time. The challenge with small-area photodetectors lies in their limited ability to absorb wavelengths near the bandgap. Due to the inherently low absorption coefficients of these wavelengths, small dimensions fail to provide sufficient propagation distance for the absorption of omnidirectional propagating modes within the semiconductor film. In contrast, enabling a uni-directional circular motion of the photons within the detector can significantly increase the effective propagation length, thereby enhancing the absorption efficiency even in a compact photodetector. The results presented here support this hypothesis, demonstrating that by promoting uni-directional circular propagation, a small-area photodetector can achieve higher absorption efficiency despite the low absorption coefficients of bandgap-near wavelengths. This approach offers a promising strategy for optimizing the performance of ultrafast photodetectors without compromising their speed and size.

#### 4. CONCLUSION

In photon-trapping (PT) photodetectors, larger planar areas enhance absorption efficiency for wavelengths near the bandgap due to the need for extended lateral propagation, which is challenging in ultrafast, small-area designs. However, promoting uni-directional circular motion within the detector can increase propagation length and absorption efficiency, offering a solution for optimizing compact photodetectors without sacrificing performance. We proposed a surface-illuminated metasurface-enabled photodetector with a deflection function and numerically demonstrated the improvement in absorption efficiency for 0.85–1.1-µm wavelengths in a silicon-based ultra-fast design. The isosceles triangular hole array metasurface caused directional scattering and improved the internal quantum efficiency for light in the wavelength range above 0.9 µm by a factor of 3.5 compared to the case without the metasurface. The enhancement is comparable to the devices that are designed with omnidirectional photon-trapping photodetectors. *Directional scattering* helps reduce the device size, ensuring ultrafast operations without sacrificing high efficiency.

## **ACKNOWLEDGMENTS**

The authors thank Ahasan Ahamed for useful discussions and help with the numerical simulations. This project was supported by a special research project (2023C-671) by Waseda University, The Center for Information Technology Research in the Interest of Society (CITRIS) and the Banatao Institute and NSF PFI-TT Award #2329884.

### REFERENCES

- 1. Bartolo-Perez, C., Qarony, W., Ghandiparsi, S., Mayet, A.S., Ahamed, A., Cansizoglu, H., Gao, Y., Ponizovskaya Devine, E., Yamada, T., Elrefaie, A.F., Wang, S.Y. and M. Saif Islam Maximizing Absorption in Photon-Trapping Ultrafast Silicon Photodetectors. *Advanced Photonics Research* **2** (2021).
- 2. Cansizoglu, H. *et al.* Dramatically Enhanced Efficiency in Ultra-Fast Silicon MSM Photodiodes Via Light Trapping Structures. *Ieee Photonics Technology Letters* **31**, 1619-1622 (2019).
- 3. Gou, J. *et al.* Rigorous coupled-wave analysis of absorption enhancement in vertically illuminated silicon photodiodes with photon-trapping hole arrays. *Nanophotonics-Berlin* **8**, 1747-1756 (2019).

- 4. Rawat, A. *et al.* Design and Fabrication of High-Efficiency, Low-Power, and Low-Leakage Si-Avalanche Photodiodes for Low-Light Sensing. *Acs Photonics* **10**, 1416-1423 (2023).
- 5. Mayet, A.S. *et al.* Finite-Difference Time-Domain Simulations of Photon-Trapping Nanohole Arrays for Enhanced Optical Absorption in Ultrahigh-Speed GaAs Photodetectors. *Acs Appl Nano Mater* **7**, 10037-10045 (2024).
- 6. Qarony, W., Mayet, A.S., Devine, E.P., Ghandiparsi, S., Bartolo-Perez, C., Ahamed, A., Rawat, A., Mamtaz, H.H., Yamada, T., Wang, S.Y. and Islam, M.S. Achieving higher photoabsorption than group III-V semiconductors in ultrafast thin silicon photodetectors with integrated photon-trapping surface structures. *Advanced Photonics Nexus* 2 (2023).
- 7. Islam, M.S. Taming photons to sense fast and faint infrared signals. *Nature Photonics* **17**, 554-555 (2023).
- 8. Ahamed, A., Rawat, A., Mcphillips, L.N., Mayet, A.S. & Islam, M.S. Unique Hyperspectral Response Design Enabled by Periodic Surface Textures in Photodiodes. *Acs Photonics* **11**, 2497-2505 (2024).
- 9. Rawat, A. *et al.* Near-infrared sensors for high efficiency and high-temperature operation enabled by ultrathin type-II quantum wells and photon-trapping structures. *Low-Dimensional Materials and Devices 2022* **12200** (2022).
- 10. Bartolo-Perez, C. *et al.* Engineering the gain and bandwidth in avalanche photodetectors. *Opt Express* **30**, 16873-16882 (2022).
- 11. Rawat, A. & Islam, M.S. Direction of Arrival Sensing Enabled by Introducing Asymmetric Surface Structures in Photodetectors. *Physics and Simulation of Optoelectronic Devices Xxxii* **12880** (2024).
- 12. Ahamad, A. *et al.* Smart nanophotonics silicon spectrometer array for hyperspectral imaging. *Conf Laser Electr* (2020).
- 13. Marsden, M. *et al.* Intraoperative Margin Assessment in Oral and Oropharyngeal Cancer Using Label-Free Fluorescence Lifetime Imaging and Machine Learning. *Ieee T Bio-Med Eng* **68**, 857-868 (2021).
- 14. Ghandiparsi, S. *et al.* High-Speed High-Efficiency Photon-Trapping Broadband Silicon PIN Photodiodes for Short-Reach Optical Interconnects in Data Centers. *J Lightwave Technol* **37**, 5748-5755 (2019).
- 15. Gao, Y. *et al.* Photon-trapping microstructures enable high-speed high-efficiency silicon photodiodes. *Nature Photonics* **11**, 301-306 (2017).
- 16. Sell, D., Yang, J.J., Doshay, S., Yang, R. & Fan, J.A. Large-Angle, Multifunctional Metagratings Based on Freeform Multimode Geometries. *Nano Lett* **17**, 3752-3757 (2017).
- 17. Zhou, Z.P. et al. Efficient Silicon Metasurfaces for Visible Light. Acs Photonics 4, 544-551 (2017).
- 18. Mikheeva, E. *et al.* CMOS-compatible all-dielectric metalens for improving pixel photodetector arrays. *Apl Photonics* **5** (2020).
- 19. Lalanne, P., Astilean, S., Chavel, P., Cambril, E. & Launois, H. Design and fabrication of blazed binary diffractive elements with sampling periods smaller than the structural cutoff. *J Opt Soc Am A* **16**, 1143-1156 (1999).
- 20. Khorasaninejad, M. *et al.* Metalenses at visible wavelengths: Diffraction-limited focusing and subwavelength resolution imaging. *Science* **352**, 1190-1194 (2016).
- 21. Tsubokawa, M. & Islam, M.S. Design of a metasurface deflector for guided absorption enhancement in a Si PIN photodiode. *Opt Express* **32**, 21121-21133 (2024).